Journal of Power Sources 672 (2026) 239620

Contents lists available at ScienceDirect

Journal of Power Sources

journal homepage: www.elsevier.com/locate/jpowsour

Effects of inhomogeneous temperature distribution during aging on the thermophysical properties of lithium-ion battery electrodes

Leonie Pfeifer *, Sabrina Herberger, Thomas Wetzel, Philipp Seegert

Karlsruhe Institute of Technology (KIT), Institute of Thermal Process Engineering (TVT), Heat and Mass Transfer, 76131, Karlsruhe, Germany

HIGHLIGHTS

- Thermophysical properties of aged NMC-LMO blend cathodes and graphite anodes.
- Particle cracking leads to a reduction of the thermal conductivity.
- SEI growth leads to a change in thermophysical properties.
- Thermal inhomogeneity during aging induces non-uniform thermophysical properties.
- Through-plane gradients have a higher impact and lead to self-reinforcing behavior.

GRAPHICAL ABSTRACT

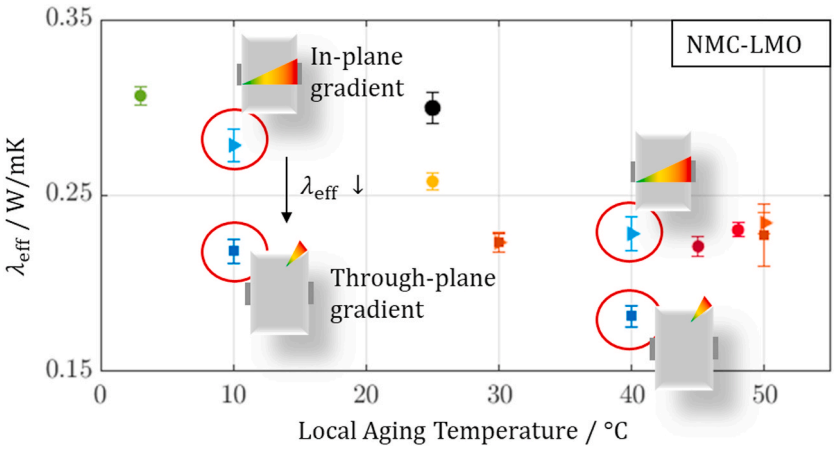

ARTICLE INFO

Keywords:
Lithium-ion battery
Aging
Thermal gradients
Thermophysical properties
Electrodes

ABSTRACT

The thermophysical properties of lithium-ion batteries are crucial for the optimized and safe design of battery thermal management systems. This paper presents an experimental investigation of aging-induced changes in the thermophysical properties of the electrodes of a commercial 20 Ah pouch cell during cyclic aging. The results show that the thermophysical properties can change significantly compared to the beginning of life, depending on the thermal aging conditions. This should be taken into account when optimizing the system design for the entire lifetime. In addition to the influence of the aging temperature, this study focuses on the influence of internal temperature inhomogeneities during aging. It can be shown that temperature inhomogeneities during aging result in inhomogeneous thermophysical properties of the electrodes and that the changes depend on the local average aging temperature, the global temperature gradient over the cell and the local temperature gradients over individual electrodes. Furthermore, it is shown that the direction of the gradient (in- or through-plane) can have a decisive impact on the changes, and thermal through-plane gradients can lead to a self-reinforcing behavior. In order to correlate the individual changes in the anode and cathode with aging mechanisms, an additional post-mortem analysis was performed.

* Corresponding author.
E-mail address: leonie.pfeifer@kit.edu (L. Pfeifer).

https://doi.org/10.1016/j.jpowsour.2026.239620
Received 1 December 2025; Received in revised form 29 January 2026; Accepted 9 February 2026
Available online 18 February 2026
0378-7753/© 2026 The Authors. Published by Elsevier B.V. This is an open access article under the CC BY license (http://creativecommons.org/licenses/by/4.0/).

Nomenclature

$\overline{T}_{Ag}$	Average local aging temperature (°C)
$\lambda_{eff,Stack}$	Effective thermal conductivity of the electrode stack (W/(mK))
λ_{eff}	Effective thermal conductivity of the electrode coating (W/(mK))
a_{Stack}	Thermal diffusivity of the electrode stack (mm^2/s)
ε	Porosity of the electrode coating (−)
$d_{Coating}$	Thickness of the coating (μm)
d_{CC}	Thickness of the current collector (μm)
d_{Stack}	Thickness of the double-sided coated electrode stack (μm)
$\rho_{Coating}$	Density of the coating (kg/m^3)
ρ_{CC}	Density of the current collector (kg/m^3)
$c_{p,Coating}$	Specific heat capacity of the coating (J/(kgK))
$c_{p,CC}$	Specific heat capacity of the current collector (J/(kgK))
A_{Stack}	Area of sample of the electrode stack (μm^2)
m_{Stack}	Mass of sample of the electrode stack (g)
ΔT_{Cell}	Global temperature difference over the cell (K)
ΔT_{Local}	Local temperature difference over the electrode sheet (K)

Abbreviations

LIB	Lithium ion battery
NMC	Nickel-manganese-cobalt-oxide
SEI	Solid electrolyte interphase
BTMS	Battery thermal management system
BoL	Begin of life
SoH	State of Health
CC	Current collector
LMO	Lithium manganese oxide
DSC	Differential scanning calorimetry
IZ	Through-plane temperature gradient aging condition
IY	In-plane temperature gradient aging condition
HS	Homogeneous stationary aging condition
EDX	Energy dispersive x-ray spectroscopy
BCB	Binder-carbon-black-phase
CEI	Cathode electrolyte interphase
SEM	Scanning electron microscopy

1. Introduction

Lithium-ion batteries (LIB) can experience a wide range of different temperatures and internal temperature distributions over the course of their operating time in electric vehicles. The temperature distribution within a cell has a strong influence on the performance and aging behavior, therefore, it is important to control the temperature distribution during operation [1,2]. A temperature of around 25 °C is optimal for most cell chemistries of LIB and minimizes the degradation effects. The performance, lifetime and safety of LIB are crucial for the automotive application, therefore, battery thermal management systems (BTMS) are applied to control the temperature and maintain an optimum operating window of the LIB. The presence of temperature gradients during aging leads to intensified and partially different aging mechanisms. Several studies demonstrate that both an in- and through-plane temperature gradient can lead to locally different aging effects depending on the local temperatures [3–6]. In the literature, the influence of the aging temperature on the aging mechanisms occurring is already established [1–3,7–9]. It is evident that the design of a BTMS plays a decisive role in the performance, aging and safety of a LIB during operation [10,11]. Knowledge of the heat release during operation and the thermal characteristics of the individual components is required to optimize the design of the BTMS [12]. The BTMS are currently mainly designed based on the data at the beginning of life (BoL). There are a few studies [12–16] that show that the thermophysical properties of the LIB change during aging and, therefore, the design of the BTMS based only on the BoL data may not be sufficient for the entire lifetime in the automotive application. In addition, the knowledge of the changes of the thermal behavior of LIB is also crucial for efficient and safe second life application of the cells.

The work of Tendera et al. [13] shows that the perpendicular thermal conductivity of a pouch cell is reduced with decreasing State of Health (SoH). The thermal conductivity was measured using a guarded hot plate method and compared for pouch cells with different SoH [13,14]. The resulting overall thermal cell behavior is, of course, decisive for the optimization of the BTMS, but the change in thermal conductivity is caused by the aging mechanisms of the individual components of the cell [10]. Since the aging mechanisms are individual for each cell chemistry, the reduction in thermal conductivity cannot be inferred exclusively from the SoH. But in addition to the overall cell behavior, an understanding of how the thermophysical properties change at the electrode level must be established in order to be able to correlate them with the aging mechanisms that occur, since the mechanisms are superimposed at the cell level and can only be partially investigated at that level, as in the work of Tendera et al. [13,14].

A consideration of the thermophysical properties at the electrode level for the anode and cathode separately is necessary in order to build up a systematic understanding of which aging mechanisms can have a critical impact on the thermal behavior of the electrodes and thus of the entire cell. The work of Spitthoff et al. [16] compares aged electrode samples with the BoL using the guarded hot plate measuring method focusing on the comparison of different aging conditions with mechanical clamping. It is shown that there is a reduction in the perpendicular effective thermal conductivity with a lower SoH.

First studies on the influence of degradation mechanisms on the thermophysical properties of the electrodes were carried out in previous work of our group in cooperation with Amy Marconnet using the laser flash method to determine the perpendicular effective thermal conductivity of aged electrodes [15]. The impact of various stationary and transient homogeneous thermal aging conditions on the thermophysical properties of the electrodes are compared. The work of Marconnet et al. [15] shows that a higher temperature during aging can lead to a lower thermal conductivity of the electrodes. An overview of comparable studies in the literature on the influence of aging on thermophysical properties is listed in Table 1.

The influence of mechanical stress and homogeneous thermal boundary conditions during aging was investigated in the few studies at the electrode level in the literature described before [15,16], but, as stated above, ideal homogeneous thermal conditions rarely occur in real application and temperature gradients develop within the cells during operation. It is evident that previous studies have not yet accounted for the influence of real inhomogeneous aging conditions, so this gap should be closed. Therefore, this study investigates the impact of inhomogeneous thermal aging conditions on the thermophysical properties of battery electrodes in addition to the impact of homogeneous thermal aging conditions. This work focuses particularly on the distinction between the impact of in- or through-plane temperature gradients during cyclic aging. The work of our group has shown that the through-plane gradient seems to be the more critical aging condition for the cell investigated from an electrochemical point of view [4,17]. The underlying aging study was performed with a commercial 20 Ah pouch cell, with a blend cathode (NMC and lithium manganese oxide (LMO)) and a graphite anode, and these cells are further investigated in this work. In this study, we examine the changes of the thermophysical properties

Table 1
Overview of work from the literature on aging effects on thermophysical properties of LIBs at the cell and electrode level [13,15,16].

	Tendera et al. [13]	Spitthoff et al. [16]	Marconnet et al. [15]
Cell level	yes	no	no
Electrode level	no	yes	yes
Investigated influencing aging factor	Impact of SoH on thermal conductivity	Impact of mechanical aging condition on thermal conductivity	Impact of homogeneous thermal aging conditions on thermophysical properties

depending on the local average aging temperature, the global temperature gradient at the cell level as well as the local temperature gradient at the electrode level. This work demonstrates the influence of temperature inhomogeneities, which can be caused, for example, by a real BTMS, and the sensitivity of the thermophysical material properties to the temperature gradient and gradient direction.

2. Experimental methodology

The thermophysical properties of electrodes (hereinafter referred to as a double-sided coated electrode stack) of aged commercial lithium-ion cells in pouch format are investigated in this work. The underlying aging study [4,17] and the experimental measurement methodology developed [18,19] for determining the thermophysical properties are part of previously published work by our group and form the basis for the investigation of the aged electrodes.

2.1. Aging study

The aged cells investigated are based on a cyclic aging study from previous work of our group, which focuses on the comparison of homogeneous and inhomogeneous thermal boundary conditions with a variation of the gradient direction in- and through-plane [4,17]. The study was performed on 20 Ah pouch cells (SPB58253172P2, Enertech International, Inc.), with a NMC111 - LMO blend cathode and a graphite anode. The thermal and mechanical aging conditions of each cell were controlled with the cell mounting used, which consists of cells that are clamped between two aluminum plates by means of springs, through which water flows as a cooling medium. The schematic structure of the cell mounting is shown in Fig. 1 a). Here it can be seen, that the use of springs allowed the pressure to be specifically set at 0.5 bar during aging. The paper by Cloos et al. [4,17] describes in detail the testing conditions and the experimental setup used to carry out the cyclic aging studies for the homogeneous and inhomogeneous thermal boundary conditions. The cells were cycled with constant current 2C between the cutoff-voltage 3.0 V and 4.2 V. An overview of the electrode samples from the cyclic aging study investigated in this work, consisting of the cell name, the respective aging condition and the SoH, is shown in Table 2. Additionally, the equivalent full cycles (EFC) of the aged cells examined in this study are shown in Fig. 1 b) with the corresponding names from Table 2.

The designation of the cells corresponds to the labeling from the aging study. Both cooling plates in the homogeneous stationary conditions are set to the aging temperature defined. In the case of the stationary in-plane gradient, the respective temperature difference is set on both sides along the cell surface. The cell has a counter-tab design, therefore, the lower temperature was applied to the side of the negative tab at each in-plane gradient for reproducibility reasons. Regarding the stationary through-plane gradient, one cooling plate was set to the lower temperature and the other to the higher temperature inducing the defined temperature difference over the thickness of the cell. The sampling positions used for the determination of the thermophysical properties are also shown in Table 2. An average local aging temperature $\overline{T}_{Ag}$ is specified for each sample position for a distinct classification. This is particularly relevant for the inhomogeneously aged cells, as there are two sampling points, one sample originates from the colder and one from the warmer region of the cell. Similar to the homogeneously aged samples, these are assigned to the respective local average temperature $\overline{T}_{Ag}$ at the sampling point. In the case of the cell IZ 10 – 40 °C, for example, a $\overline{T}_{Ag}$ of approximately 10 °C is assumed for the sampling point on the part of the cell with the colder boundary condition.

2.2. Measurement methodology and sample preparation

A measurement method to determine the thermophysical properties on the electrode level is used in this work which consists of measuring the specific heat capacity and density of the current collector (CC) and electrode coating as well as measuring the thermal diffusivity of the electrode stack (double-sided coated CC). The measurement methodology was developed and established in previous work in our group by Oehler et al. [18,19]. The effective thermal conductivity $\lambda_{eff,Stack}$ of the electrode stack is calculated using the following equation.

$$\lambda_{eff,Stack} = a_{Stack} \cdot \left((1-\varepsilon) \cdot \frac{d_{Coating}}{d_{Stack}} \cdot \rho_{Coating} \cdot c_{p,Coating} + \frac{d_{CC}}{d_{Stack}} \cdot \rho_{CC} \cdot c_{p,CC} \right) \tag{1}$$

This requires the measurement data of the thermal diffusivity a of the electrode stack, the density ρ and specific heat capacity c_p of the coating and the CC. In addition, the porosity of the coating ε and the thicknesses of the electrode stack d_{Stack} and CC d_{CC} must be measured. Sample

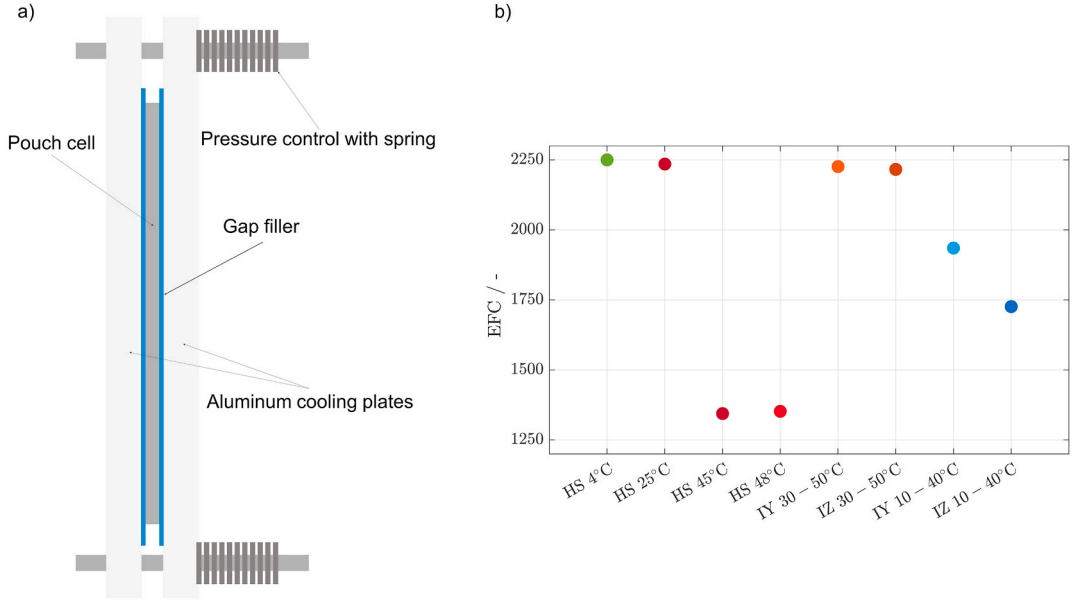

Fig. 1. a) Schematic cross-sectional view of the cell mounting with the pouch cell b) Overview of the final equivalent full cycles (EFC) of the various aged cells that form the basis for this work [20].

Table 2
Overview of the aged pouch cells [4,17] and prepared samples for the investigation of the thermophysical properties in this work.

Cell name	Aging condition	SoH	Samples	$\overline{T}_{Ag}$
BoL	none	100 %	BoL | Cathode	25 °C
			BoL | Anode	25 °C
HS 4 °C	4 °C homogeneous	85.9 %	HS 4 °C | Cathode	4 °C
				4 °C
			HS 4 °C | Anode	
HS 25 °C	25 °C homogeneous	85.8 %	HS 25 °C | Cathode	25 °C
				25 °C
			HS 25 °C | Anode	
HS 45 °C	45 °C homogeneous	67 %	HS 45 °C | Cathode	45 °C
				45 °C
			HS 45 °C | Anode	
HS 48 °C	48 °C homogeneous	53 %	HS 48 °C | Cathode	48 °C
				48 °C
			HS 48 °C | Anode	
IY 30 – 50 °C	30 – 50 °C in-plane gradient	69.7 %	IY 30 – 50 °C | Cathode	30 °C
				50 °C
			IY 30 – 50 °C | Cathode	30 °C
				50 °C
			IY 30 – 50 °C | Anode	
			IY 30 – 50 °C | Anode	
IZ 30 – 50 °C	30 – 50 °C through-plane gradient	66.8 %	IZ 30 – 50 °C | Cathode	30 °C
				50 °C
			IZ 30 – 50 °C | Cathode	30 °C
				50 °C
			IZ 30 – 50 °C | Anode	
			IZ 30 – 50 °C | Anode	
IY 10 – 40 °C	10 – 40 °C in-plane gradient	79.8 %	IY 10 – 40 °C | Cathode	10 °C
				40 °C
			IY 10 – 40 °C | Cathode	10 °C
				40 °C
			IY 10 – 40 °C | Anode	
			IY 10 – 40 °C | Anode	
IZ 10 – 40 °C	10 – 40 °C through-plane gradient	82.1 %	IZ 10 – 40 °C | Cathode	10 °C
				40 °C
			IZ 10 – 40 °C | Cathode	10 °C
				40 °C
			IZ 10 – 40 °C | Anode	
			IZ 10 – 40 °C | Anode	

preparation in this work proceeded as follows. The aged pouch cells were discharged to a state of charge (SoC) of 0 % and opened in a glovebox under an argon atmosphere and the electrode sheets were washed in dimethyl carbonate and allowed to evaporate afterwards. A variation of the degree of intercalation is not performed in this work, all samples were taken at a SoC of 0 %. The measurement of the specific heat capacity and density are performed separately for the CC and the electrode coating. For this purpose, the coating is measured in powder form. This is possible because the specific heat capacity and density depend solely on the mass fractions of the components contained. When measuring the thermal diffusivity, the sample is punched directly from the electrode sheet, thus taking into account the influence of the microstructure, as this parameter depends on it.

The determination of the specific heat capacity was carried out using differential scanning calorimetry (DSC). The devices used are a DSC Q2000 (TA Instruments) and Discovery DSC 2500 (TA Instruments). The electrode coating and the CC material were measured separately by scraping the electrode coating off the CC and subsequently filling and pressing the powder into the DSC pan under an argon atmosphere. Similar to the measurement of the specific heat capacity, the density was determined separately for the electrode coating and the CC material at a temperature of approximately 25 °C. The sample materials were then measured using a gas pycnometer Micro-Ultrapy-1200e (Quantachrome). The density is calculated using the determined volume and mass of the sample. The mass is determined using an analytical balance XPE206 Delta Range (Mettler Toledo).

The through-plane thermal diffusivity was measured using the laser flash method with a Hyperflash 467 (NETZSCH). A foil sample holder was used and the electrodes were punched out using a handheld electrode punch (NOGAMI) with a diameter of 25 mm. The measurement of the thermal diffusivity in the laser flash was performed under a helium atmosphere. With a thermal conductivity of around 0.14 W/(mK) [21] helium shows a quite similar thermal conductivity to conventional electrolyte systems, which is around 0.16 W/(mK) [22]. This enables helium, as a measuring gas, to emulate the thermal conductivity of the electrolyte in the pore space very well and enables a very good approximation of the thermal behavior of electrolyte-soaked electrodes, as has already been shown by Oehler et al. [18,19]. A temperature range from −20 to 60 °C was measured at 10 K intervals. The penetration model in the evaluation software provided by NETZSCH was used for evaluation [23]. The measurements were performed at ambient pressure, and no variation study of the pressure influence was conducted as part of this work.

The thickness of the electrode stacks was determined using a mechanical gauge (Mahr Micromar 40 EWR). Different measurement methods were investigated regarding the porosity and compared as part of this work. The porosity derived from mercury porosimetry (BELPORE MICROTRAC) measurement data was compared to the gravimetrically determined porosity based on the thickness and density measured. For this purpose, several samples with a diameter of 25 mm per aging condition were weighed with an analytical balance for determining the mass of the sample m_{Stack} and the porosity was calculated with the area of the sample A_{Stack} using equation (2).

$$\varepsilon = \frac{A_{Stack} \cdot d_{Coating} - \frac{(m_{Stack} - A_{Stack} \cdot d_{CC} \cdot \rho_{CC})}{\rho_{Coating}}}{A_{Stack} \cdot d_{Coating}} \tag{2}$$

The results of the thermal characterization of the aged electrode samples according to the methodology described are presented and discussed in the following in the context of an additional post-mortem analysis to link the changes of the thermophysical properties to possible aging effects. The uncertainty of the measurements was calculated according to the Guide to the Expression of Uncertainty in Measurement using a type A uncertainty analysis. For this purpose, several samples were measured for each aging condition in order to be able to carry out a statistical evaluation [24].

3. Results

In order to investigate the influence of inhomogeneous thermal conditions during aging on the thermophysical behavior of the electrodes, the experimental parameters analyzed are presented in the following section. The parameters for determining the perpendicular effective thermal conductivity of the electrode stack are evaluated separately for the anode and cathode.

3.1. Porosity

The change of the electrode porosity over the course of aging has not been widely investigated or systematically discussed in the literature. However, this parameter is of central importance for the calculation of the effective thermal conductivity. The results of the gravimetric porosity of the electrode coating of the various samples of the aged cells are shown in Fig. 2 and compared to the values of the cell at BoL. The porosity is plotted over the local aging temperature $\overline{T}_{Ag}$. The individual sample positions and aging conditions correspond to the assignment in Table 2. The density and stack thickness of each sample is measured for the calculation of the porosity and shown in the supplementary

information in Fig. S1. Fig. 2 a) shows the gravimetrically determined porosities of the cathode stacks. It can be seen that the porosity of the cathode coating increases at a higher $\overline{T}_{Ag}$ for all different aging conditions. The same trend can be seen for the porosity as for the thickness and the density. A distinct difference in porosity is visible for the in- and through-plane gradients with the temperature difference of 10 – 40 °C which underlines the inhomogeneous changes occurring.

In addition, mercury porosimetry was carried out on selected samples to assess the pore size distribution, as this provides a decisive indication of the underlying microstructure. The results of the mercury porosimetry confirm the results of the gravimetric porosity measurements. The pore size distribution of a BoL cathode is compared with the HS 48 °C cathode in the supplementary information in Figure S 2 a). It can be seen that the distribution shifts toward smaller pores for the aged cathode.

The change in porosity of the anode during aging shows a reduction in most samples. A remarkably high porosity on the 30 °C side can be observed only in case of the IY 30 – 50 °C aging condition, which correlates with the corresponding higher thickness values. When comparing the pore size distribution of the aged anode coating to the BoL (exemplified in Figure S 2 b), it can be seen that there is no significant change.

3.2. Specific heat capacity, thermal diffusivity and effective thermal conductivity

The results of the specific heat capacity, thermal diffusivity and effective thermal conductivity of the BoL cell and the homogeneously aged cells are shown in the supplementary information in Figure S3. The respective parameters are plotted against the temperature of the measurement between −20 and 60 °C. The measurement at different temperatures is important, as some thermophysical properties show a strong temperature dependence. The results show that the impact of aging on the individual temperature dependency of the thermal parameters in this study can be considered to be very low and one chosen measurement temperature point is representative for the relative comparison. To investigate the influence of the different thermal aging conditions on the thermophysical properties of the anode and cathode, the following results of the measurements are presented only for the measuring temperature of 20 °C.

The results of the specific heat capacity, thermal diffusivity and effective thermal conductivity are plotted in Fig. 3 over the local average aging temperature $\overline{T}_{Ag}$, separately for cathode and anode samples, analogous to the previous results following the classification in Table 2.

Only minor changes for the homogeneously and inhomogeneously aged cells can be seen compared to the BoL for the specific heat capacity of cathode (Fig. 3 a) and anode coating (Fig. 3 b). For the inhomogeneously aged cells, it can be seen that the gradient direction has a different impact for both anode and cathode in case of the temperature difference between 10 and 40 °C. The through-plane gradient leads to a stronger reduction of the specific heat capacity compared to the in-plane gradient. This influence is not significantly visible in the case of the temperature gradients with temperature differences between 30 and 50 °C.

In contrast to the results of the specific heat capacity, the results of the thermal diffusivity show changes for the aged cells in comparison to the BoL. In the case of the cathode stack, shown in Fig. 3 c) for the homogeneous aging conditions, it can be seen, that the thermal diffusivity is more reduced for higher aging temperatures $\overline{T}_{Ag}$. The values of the thermal diffusivity of the inhomogeneously aged cathode stacks confirm the trend regarding the impact of $\overline{T}_{Ag}$ observed for the homogeneously aged samples. In the case of the in- and through-plane gradients with a temperature difference between 10 and 40 °C, it can be seen that inhomogeneous changes can occur within a cell. The respective sample with the locally higher aging temperature shows a lower thermal conductivity. The overall reduction is more pronounced in the case of the through-plane gradient IZ 10 – 40 °C. No significant inhomogeneities are visible for the in-plane and through-plane temperature gradients with a temperature difference between 30 and 50 °C. All thermal diffusivities of the homogeneous and inhomogeneous samples above $\overline{T}_{Ag}$ of 30 °C are almost at the same level, with the exception of the sample at $\overline{T}_{Ag}$ of 40 °C of the through-plane gradient IZ 10 – 40 °C. In

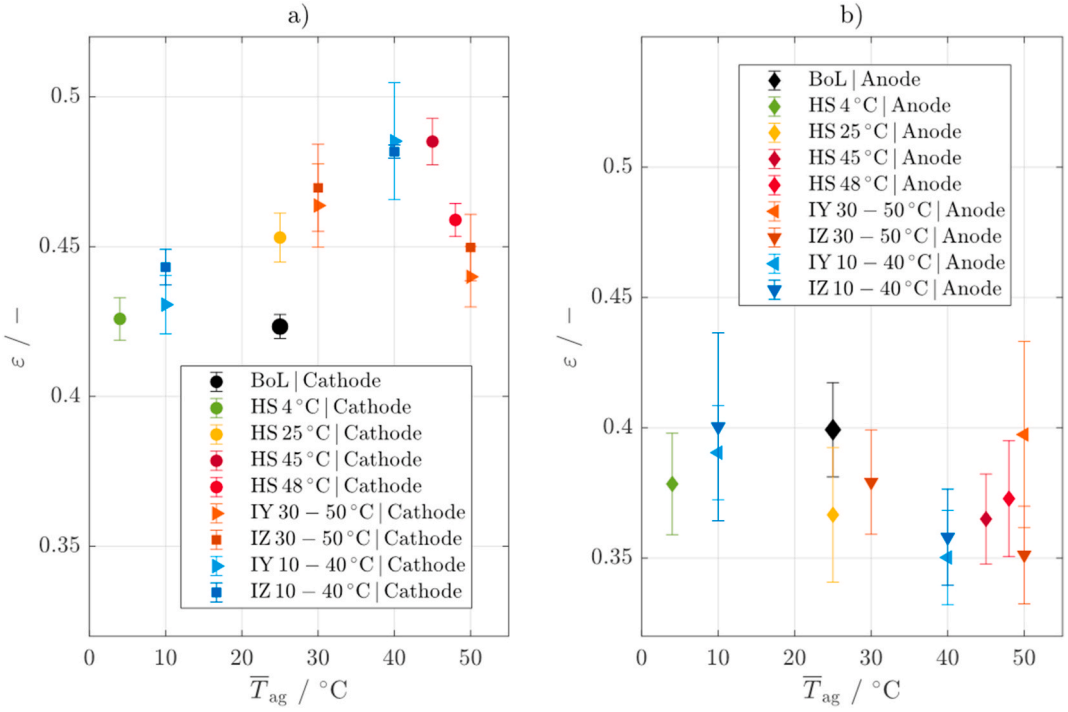

Fig. 2. Comparison of the porosity of the electrodes of the cell at the BoL with the electrodes of the aged cells for the different homogeneous and inhomogeneous thermal aging conditions. The porosity of a) cathode and b) anode are shown over the local average aging temperature $\overline{T}_{Ag}$ of the samples.

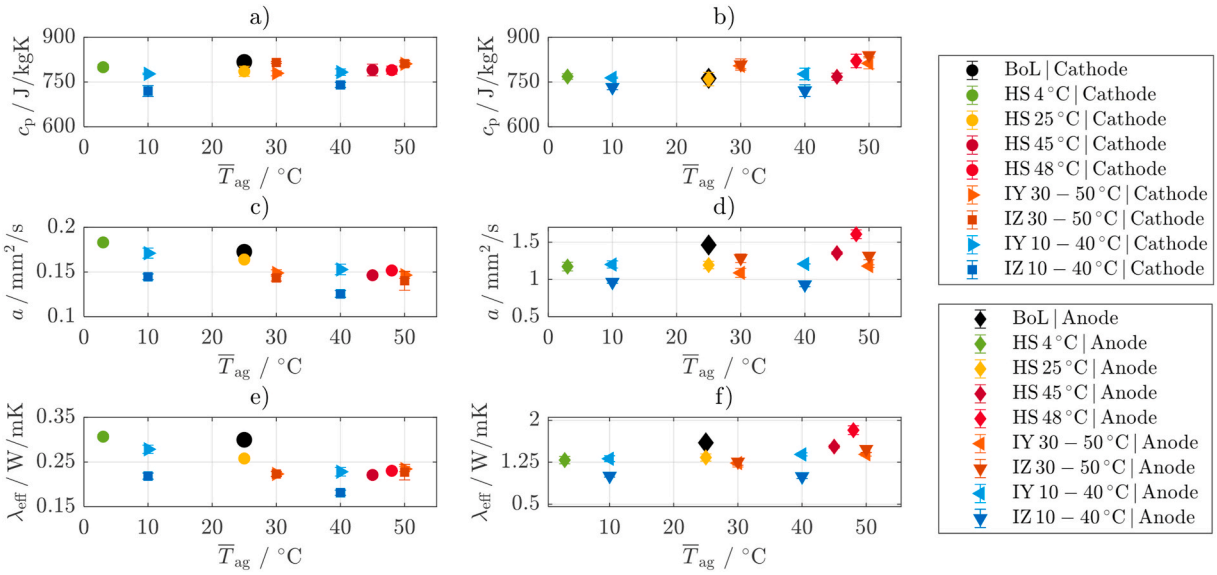

Fig. 3. Comparison of the data of the electrode of the BoL cell with the electrodes of the homogeneously and inhomogeneously aged cells. The specific heat capacity a) of the cathode coating and b) the anode coating, the thermal diffusivity c) the cathode stack and d) the anode stack and the effective thermal conductivity of e) cathode coating and f) anode coating for a measurement temperature of 20 °C are shown. In each case, the data is shown above the local average aging temperature of the individual samples.

principle, an increase in temperature during aging does not appear to cause a general linear reduction in thermal diffusivity above an aging temperature of 30 °C. The anode stacks in Fig. 3 d) show a contrary behavior. Here, the thermal diffusivity is more reduced for lower aging temperatures $\overline{T}_{Ag}$ in comparison to the BoL values. Contrary to the cathode stack, the development of inhomogeneous thermophysical properties in the anode is more pronounced at the aging condition with a temperature difference from 30 to 50 °C than 10 – 40 °C. The inhomogeneity within the anode is greater in case of the through-plane gradients than the in-plane gradients of 30 – 50 °C. Fewer inhomogeneities can be observed for the temperature gradients of IZ and IY 10 – 40 °C, but a clear difference between in-plane and through-plane gradients is detectable. Analogous to the cathode, the through-plane gradient leads to a more pronounced reduction in the thermal diffusivity. Accordingly, a higher aging temperature at the cathode leads to a greater reduction in thermal diffusivity, while a lower aging temperature at the anode leads to a greater reduction.

The effective thermal conductivity of the electrode stacks is calculated according to equation (1). It can be seen in Fig. 3 e) that the effective thermal conductivity of the aged cathode coating is more significantly reduced at higher than at lower aging temperatures $\overline{T}_{Ag}$. A clear trend is visible here as a function of the aging temperature given. In the case of the cells IZ and IY 10 – 40 °C, inhomogeneous material properties can be detected. The impact of the gradient direction on the effective thermal conductivity is the same as for the thermal diffusivity. In the case of the anode in Fig. 3 f), in accordance with the results of the thermal diffusivity, the impact of the aging temperature is contrary to the behavior of the cathode stacks. The highest $\overline{T}_{Ag}$ leads to a minimal reduction of the effective thermal conductivity.

4. Discussion

In order to classify and interpret the influence of the inhomogeneous thermal aging conditions on the thermophysical properties of the electrodes, the results of the homogeneously aged samples are first discussed and then compared with the ones for inhomogeneous thermal boundary conditions.

The results shown are classified in Table 3 within the context of the literature, for both BoL and end of life values. However, it should be noted that each electrode has a different configuration and that cell chemistry also has a decisive influence on thermal conductivity. Therefore, a comparison can only be made with similar cell chemistries.

4.1. Homogeneous aging condition

As has already been described in chapter 3.2, the changes of the thermophysical material properties of aged cathodes and anodes depend on the aging temperature. As part of the additional post-mortem-analysis in this work, scanning electron microscopy (SEM) images of cross-sections of the cathode and anode stack were investigated to identify possible changes within the microstructure of the electrodes. The SEM images are shown in Fig. 4.

Based on the homogeneously aged samples in Fig. 3 e), it is evident that a higher aging temperature $\overline{T}_{Ag}$ leads to a reduction of the thermal conductivity for the cathode stack. The images of the BoL cathode stack in Fig. 4 a) and the zoom on the coating in Fig. 4 b) show that an intact binder-carbon-black-phase (BCB) and intact secondary particles of the NMC and LMO are present in the BoL state of the cell. By comparison, SEM images of the cross-section of the cathode at the aging condition HS 48 °C are shown in Fig. 4 c). A slight delamination in the middle of the cathode coating can be observed. Friesen et al. [26] report delamination

Table 3
Comparison of measured data of the through-plane thermal conductivity with literature data from Steinhardt et al. [25] and Spitthoff et al. [16], the electrode soaked with electrolyte.

	Steinhardt et al. [25]	Spitthoff et al. [16]	This work
NMC (BoL)	0.55 – 0.90 W/(mK)	0.89 W/(mK)	–
NMC (aged)	0.54 ± 0.02 W/(mK)	0.71 W/(mK)	–
NMC-LMO (BoL)	–	–	0.30 ± 0.01 W/(mK)
NMC-LMO (aged)	–	–	0.18 – 0.30 W/(mK)
Graphite (BoL)	0.36 – 1.50 W/(mK)	1.27 – 1.93 W/(mK)	1.59 ± 0.02 W/(mK)
Graphite (aged)	0.62 ± 0.02 W/(mK)	1.34 W/(mK)	0.99 – 1.53 W/(mK)

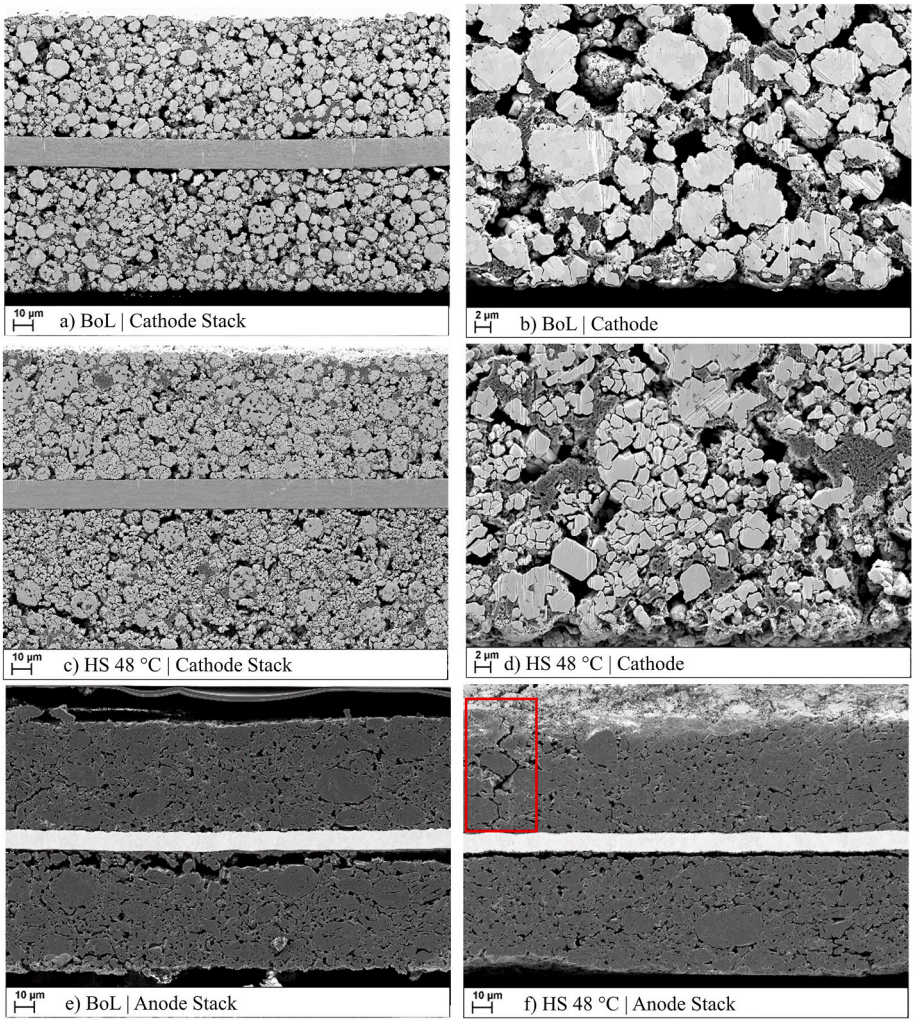

Fig. 4. SEM images of the cross-section of the cathode and anode of the BoL and HS 48 °C cell: a) BoL cathode stack, b) BoL cathode coating, c) HS 48 °C cathode stack, d) HS 48 °C cathode coating, e) BoL anode stack and f) HS 48 °C anode stack with crack highlighted.

of the cathode coating of the CC during aging, which is not visible in the SEM images in Fig. 4 a) – d). However, it was observed during the cell opening process that entire areas of the cathode coating detached from the CC without external mechanical impact. This was the case for the cells subjected to homogeneous temperature HS 45 °C and HS 48 °C, as well as for the cells aged under inhomogeneous temperature distribution. In the case of the inhomogeneously aged cells the cathode samples at the higher $\overline{T}_{Ag}$ showed the behavior described.

In addition, an extreme degree of particle cracking for the cathode of HS 48 °C is visible in Fig. 4 c) and d), which is more reminiscent of complete fragmentation. This degree of particle cracking is more severe than that described in the literature [27–29]. Based on the results of energy dispersive x-ray spectroscopy (EDX) of the cross-sections, it can be assumed that particle cracking only occurs in NMC, while LMO continues to show completely intact particles. Fig. 4 d) shows a close-up of the particle fragmentation of NMC secondary particles at HS 48 °C. It can also be seen here that the solid connection from the active material particles with the BCB phase is damaged by the complete fragmentation of the particles, similar to reports in the literature [30]. Each new surface after particle cracking can lead to a reaction with the electrolyte and results in changes of the microstructure [8]. The comparatively more conductive heat transfer paths within the solid phase are reduced due the delamination within the layer, extensive particle fragmentation and associated reduced contact surface of the BCB-phase. Although several individual particles are still present, the solid interconnection within the secondary particles is partially missing. Particle pulverization is usually observed at voltages higher than 4.5 – 4.7 V [31,32].

One possible explanation could be that the mechanical stability of the binder phase is reduced due to the high aging temperature. Polyvinylidene fluoride for example shows a higher flexibility at temperatures around 60 °C [26,33]. The increased flexibility of the binder at elevated temperatures may facilitate a greater spatial separation of particle fragments. This effect is probably driven by volumetric changes during intercalation and deintercalation processes, ultimately rendering the original secondary particle structure unidentifiable. Such behavior could explain the pronounced fragmentation observed. The exact composition of the BCB-phase is not known for this cell, but it is evident that the changes in the BCB-phase during aging should also be taken into account to understand the changes in the microstructure. The results also explain the changed pore size distribution in the case of the HS 48 °C cell. The fragmentation creates the shift to smaller pores and produces a higher overall layer thickness due to the changes in the microstructure. Additionally, the new surface of the fragmented particles enables the formation of new cathode electrolyte interfaces (CEI) [32]. By contrast the effect of particle cracking is less pronounced at lower aging temperatures, as is CEI formation [8]. This can be correlated with the results measured in this work and seen in the lower stack thickness in the case of the HS 4 °C and HS 25 °C cells. This may also explain the less pronounced reduction of the effective thermal conductivity in these cases with lower aging temperatures.

The influence of the SoH on the effective thermal conductivity can be investigated through the comparison of the results of HS 45 °C and HS 48 °C. The HS 45 °C cell has a SoH of 67 %, while the HS 48 °C cell has a SoH of 53 %, as described in Table 2. The effective thermal conductivity of the two cathode samples is almost the same. This does not correspond directly to the results of Tendera et al. [13] at cell level and shows that the SoH does not offer a standalone option for assessing changes in the thermophysical properties the specific aging conditions must be taken into account.

On the anode side, the results in chapter 3.2 show a reduction of the effective thermal conductivity for lower $\overline{T}_{Ag}$. At a higher $\overline{T}_{Ag}$ increased SEI growth occurs on the anode side [34,35]. Due to the organic components of the SEI, it will not feature a comparably high thermal conductivity, but the increased SEI formation [15] and the associated slight reduction in porosity can increase the number of solid heat conduction paths, thereby improving the overall thermal conductivity. Manganese was detected on the surface of the anode for the two anode samples at higher $\overline{T}_{Ag}$ (HS 45 °C [4] and HS 48 °C), using EDX. Thus, the crosstalk between the cathode and anode is proven at these aging conditions, which according to the literature can enhance the SEI formation [36, 37].

A cross-section of the anode stack at BoL is shown in Fig. 4 e). The SEM image shows that even in the case of the BoL cell, partial delamination on one side of the copper CC can occur. It appears that in these cases the connection via the BCB-phase is no longer stable even in the BoL state. By comparison, Fig. 4 e) and f) show that an almost complete one-sided delamination occurs for the HS 48 °C cell and that in addition cracks within the microstructure are present over the height of the anode coating. Such cracks have been reported by Chen et al. [38] and explained by the failure of the binder. These changes of the microstructure lead to a reduction of heat conduction paths and, thus, explain the reduction of the effective thermal conductivity.

A possible effect for the reduction of the effective thermal conductivity for a lower $\overline{T}_{Ag}$ such as in the case of the HS 4 °C cell, could be the increased formation of cracks within the graphite coating due to lower aging temperatures. In contrast to the more flexible binder at high temperatures, which can allow the particle fragments to shift on the cathode side, cracks could occur more severely at lower temperatures due to the lower flexibility of the binder [38] resulting in higher mechanical stress within the anode during the volume changes associated with charging and discharging.

4.2. Inhomogeneous aging condition

In order to systematically analyze the complex influence of inhomogeneous temperature distributions on the aging-induced changes in thermophysical properties, three different levels of impact are defined in this work at which the effects of inhomogeneous temperature distributions within a cell manifest themselves. A schematic overview of these three levels is illustrated in Fig. 5 a) for the example of the through-plane gradient over the cell from the first (C1) to the last cathode sheet (C18). The first level of impact is the local aging temperature $\overline{T}_{Ag}$. This parameter has already been defined for the clarification of the samples and enables a comparison with the results of the study of the homogeneously aged cells. In the latter a single uniform $\overline{T}_{Ag}$ prevails. By contrast, inhomogeneously aged cells have a non-uniform internal temperature distribution induced by the global temperature gradient imposed externally, resulting in a temperature difference ΔT_{Cell} over the cell. This global temperature gradient over the cell is the second level of impact, which takes into account the magnitude and the direction of the gradient. The third level introduces the local temperature gradient, which is linked with the temperature difference ΔT_{Local} over the thickness of the individual electrodes within the aged cell. All three levels cannot be considered independently of each other and result from the inhomogeneous temperature distribution, offering the opportunity to analyze the various effects in a more targeted manner. In the case of a real application within an electric vehicle the BTMS can induce a global temperature gradient with a ΔT_{Cell}. The combination of the heat release within the cells and the BTMS leads to an inhomogeneous internal temperature distribution, which can also be divided for the analysis into the three levels of impact.

As has already been observed in the homogeneous thermal aging conditions and the literature [15], the local aging mechanisms, that depend on the local aging temperature $\overline{T}_{Ag}$ influence the changes of the thermophysical properties. The inhomogeneous thermal aging conditions of the underlying aging study investigated cover the range ΔT_{Cell}

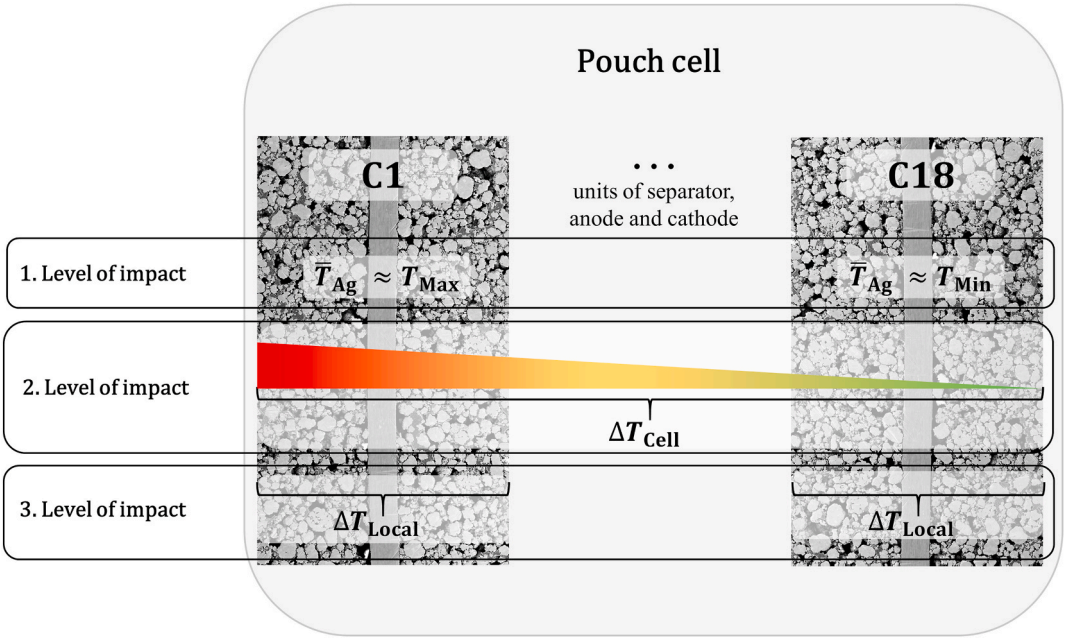

Fig. 5. Overview of the three levels of impact for one example with a through-plane temperature gradient. 1. level of impact: local aging temperature $\overline{T}_{Ag}$, 2. level of impact: global temperature gradient with ΔT_{Cell} over the complete cell and 3. level of impact: local temperature gradient with ΔT_{Local} over the individual electrodes.

from 10 to 40 °C and also from 30 to 50 °C with the gradient directions of in- and also through-plane. Based on the literature, the through-plane gradient can be the gradient direction with a more serious scope of impact considering aging [4,5]. The results of the underlying aging study show that differences in the gradient direction occur only for the gradient with ΔT_{Cell} 30 – 50 °C [4]. For the gradient with ΔT_{Cell} between 10 and 40 °C, no significant difference of the aging behavior on the performance in the form of capacity loss can be observed between both directions of the gradient. Due to the through-plane gradient there is a temperature gradient on the electrode level between the anode and the counter cathode. Such local gradients can impact the aging behavior and result in differences in the overpotential behavior and effective capacity of the electrodes, as shown by Carter et al. [5,39].

4.2.1. Through-plane temperature gradient

Firstly, the results for the cathode stack and the effect of the through-plane gradient will be discussed. The gradient with a ΔT_{Cell} of 30 – 50 °C leads to an almost homogeneous reduction in the effective thermal conductivity for both gradient directions. The effective thermal conductivity in both gradient directions is at the same level as the results of the HS 45 °C and HS 48 °C. The thermal gradient with a ΔT_{Cell} of 10 – 40 °C leads to inhomogeneous thermophysical properties and shows a dependency of the gradient direction. The through-plane gradient leads to a significantly reduced thermal conductivity of the cathode compared to the in-plane gradient. The according SEM images are shown in Fig. 6 a) to b) for the cell IZ 10 – 40 °C. The local differences in the microstructure between the sample position on the warm side of $\overline{T}_{Ag}$ = 40 °C (Fig. 6 a) and on the cold side of $\overline{T}_{Ag}$ = 10 °C (Fig. 6 b) for the through-plane gradient are displayed.

As has already been described in the case of the homogeneous cells, a higher $\overline{T}_{Ag}$ leads to increased particle cracking. It is clearly visible in the SEM images of the IZ 10 – 40 °C in Fig. 6 a) and b), that particle cracking is more pronounced in the sample at $\overline{T}_{Ag}$ = 40 °C, while particle cracking also occurs at the lower $\overline{T}_{Ag}$ of 10 °C, but the original shape of the NMC particles is still recognizable. When comparing the samples with the SEM results of the HS 48 °C cell, a significantly stronger change in the microstructure can be seen in the case of the through-plane gradient.

After the discussion of the impact of $\overline{T}_{Ag}$, the second level of impact focuses on the influence of the gradient at the cell level with ΔT_{Cell}. It can be seen in the work of Paarmann et al. [40], that a temperature gradient leads to a different current distribution within a parallel connection of cells, which is also the case for the parallel connected electrode sheets within a cell stack. The electrodes with a higher temperature experience a higher current density and thus a higher mechanical load on the active material particles [40]. This effect possibly intensifies the particle cracking due to the already higher temperature at the sample position $\overline{T}_{Ag}$ of 40 °C. A temperature difference of ΔT_{Cell} = 30 K is applied externally for the IZ 10 – 40 °C, by comparison, the difference for the IZ 30 – 50 °C is only 20 K. The non-uniform current distribution is probably less pronounced in the case of IZ 30 – 50 °C due to the smaller temperature gradient and as the changes in resistance as a function of temperature are smaller at higher temperatures [41], the inhomogeneity of the current load is less pronounced [40].

However, the local temperature gradient with ΔT_{Local} as the last level of impact must also be considered in order to obtain a complete analysis. ΔT_{Local} over the electrode has an additional impact on the aging behavior and is caused by ΔT_{Cell}. Aging phenomena such as delamination are described in the literature regarding through-plane gradients [5]. Such delamination effects can be seen pronounced on both samples ($\overline{T}_{Ag}$ = 40 °C and $\overline{T}_{Ag}$ = 10 °C) in the SEM of the cross-sections in Fig. 6 a) and b). In addition to the fragmentations and particle cracking, a difference can be seen between the two coating sides within the individual cathode stacks of the IZ 10 – 40 °C cell. In each case, one side of the cathode shows significantly stronger delamination within the coating than the other. The literature reports, that through-plane thermal gradients can induce such degradation mechanism. It is decisive here which coating side of the cathode has a colder opposite anode coating and which has a warmer anode coating counterpart [5,42]. According to Carter et al. [5], this leads to stronger plating and pore clogging for the colder anode, and to particle cracking and delamination on the corresponding cathode side.

The ΔT_{Local} depends not only on the externally induced gradient over the cell, but also on the thermophysical properties of the individual electrodes. This work investigates the influence of changes in the thermophysical properties on the distribution of the individual ΔT_{Local} over the cell stack. The calculation of the temperature differences across the layers is carried out one-dimensionally according to equation (S1) described in the supplementary information chapter 3 by Krischer et al. [43]. Regarding both electrodes, the thermal conductivities and thicknesses measured were used depending on the configuration described, for the layer thickness and the thermal conductivity of the pouch foil data from previous work from our group of this cell is used, as well as the thermal conductivity of the separator from the literature [44] and the thickness measured from Ref. [45]. The results of the distribution of ΔT_{Local} over the cell for IZ 10 – 40 °C and IZ 30 – 50 °C are shown in the supplementary information in Figure S 4.

The changes of the thermophysical properties measured during aging are taken into account for the calculation of ΔT_{Local}, especially the inhomogeneous thermophysical material properties. Regarding qualitative comparison, a linear progression of the thermophysical properties over the sheets was assumed in the case of the inhomogeneous thermophysical properties of the electrodes between the two sampling points of maximum and minimum temperature measured. The calcula-

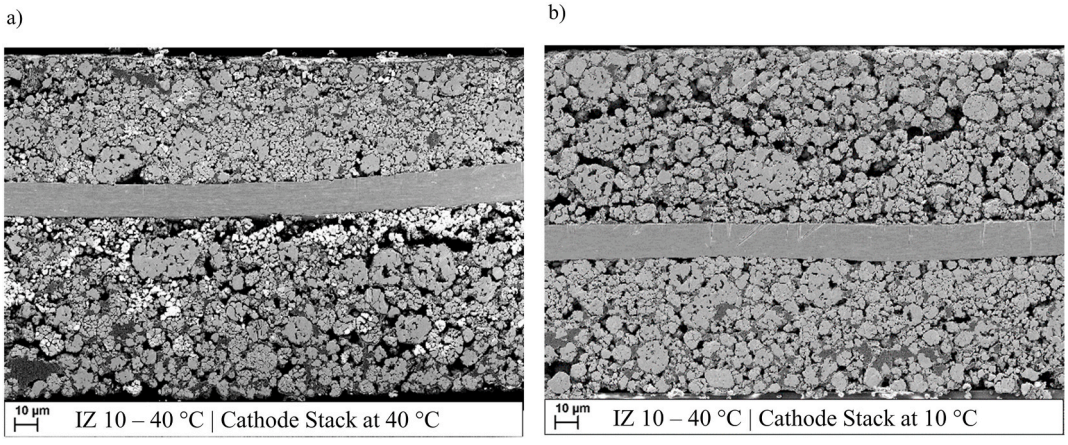

Fig. 6. SEM images of the cross-section of cathode of IZ 10 – 40 °C a) IZ 10 – 40 °C cathode stack at 40 °C, b) IZ 10 – 40 °C cathode stack at 10 °C.

tion with inhomogeneous thermophysical material properties in Fig. 3 shows, that there is an increase of the ΔT_{Local} for the cathode stacks on the side of $\overline{T}_{Ag} = 40$ °C and a reduction on the side of $\overline{T}_{Ag} = 10$ °C.

This results in a reinforcing effect: the higher ΔT_{Cell} is, the higher the ΔT_{Local} over the individual electrodes and, therefore, a higher stress on the respective electrode is induced. The different aging effects occurring at IZ 10 – 40 °C | 10 °C and IZ 10 – 40 °C | 40 °C within the same cell are not only caused by the different $\overline{T}_{Ag}$, but can also be intensified in the course of the aging by the development of inhomogeneous thermophysical material properties and the resulting different ΔT_{Local} across the individual cathodes and anodes with a constant ΔT_{Cell}. The gradient across the electrode is higher in the case of IZ 10 – 40 °C and the effects on the thermophysical material properties of the cathode are accordingly higher compared to the results of IZ 30 – 50 °C.

A closer look at the anode shows that the through-plane gradient at IZ 10 – 40 °C leads to a greater inhomogeneity of the thermophysical properties. In principle, the influence of $\overline{T}_{Ag}$ on the anode shows the opposite trend to the cathode and a lower $\overline{T}_{Ag}$ leads to lower thermal conductivities. This behavior is also confirmed for the inhomogeneous cells. The three levels of impact introduced are also superimposed in the case of the anode. The local gradient over the anode stacks with ΔT_{Local} can lead to increased SEI growth, pore clogging, delamination and plating, as shown in literature [5,42]. The increased SEI formation at the higher $\overline{T}_{Ag}$ at IZ 30 – 50 °C contributes to an increase of the heat conduction paths, as a result of which the effective thermal conductivity is higher at the higher $\overline{T}_{Ag}$ compared to the lower aging temperature. The through-plane temperature gradient also shows extensive plating on the anode coating side with a warmer cathode counterpart. In this work, samples were taken from the plating area and compared with anodes without plating. No significant influence of the plating on the effective thermal conductivity could be found, this result confirms the work of Tendera et al. [13] and Marconnet et al. [15].

The more critical aging mechanism for the anode is the change of the microstructure. It is noticeable observing the electrode surface of the IZ 30 – 50 °C using light microscopy that different colors can be seen (Fig. S5 in the supplementary information). Increased SEI formation can be seen at the higher local aging temperature, as well as lithium-rich deposits analogous to HS 45 °C and HS 48 °C. The SEI probably has a lower thermal conductivity than the graphite coating, based on the organic components [15], but strong SEI formation leading to the development of new solid pathways can also compensate for the loss of heat conduction paths. In the case of IZ 10 – 40 °C, different colorations of the anode can also be seen when comparing the two samples at maximum and minimum local aging temperature $\overline{T}_{Ag}$. However, in comparison to IZ 30 – 50 °C, other discolorations are visible in the higher temperature range. These colorations in case of ΔT_{Cell} of 10 – 40 °C correspond to the degree of lithium intercalation present in the graphite structure, as mentioned in the literature [46]. As the electrodes theoretically have time before cell opening for complete relaxation [47], this coloration can occur due to island formation of the anode [9,48]. Burow et al. showed that different degrees of lithium intercalation can be present in aged cells after cell opening [49]. This leads to the conclusion that certain parts of the microstructure are no longer electrochemically connected to the rest of the electrode. Such interruptions can have an influence on the thermophysical properties and reduce the thermal conductivity by reducing heat conduction paths. The through-plane temperature gradient can lead to contact losses in the network of the anode material [5].

4.2.2. *In-plane temperature gradient*

In comparison to the results of the through-plane gradients the analysis of the in-plane gradient shows local differences, but the imposed outer temperature difference ΔT_{Cell} does not lead to an increase of ΔT_{Local} due to changes in the through-plane thermal conductivity of the electrodes during the aging. In the case of parallel thermal conductivity, the influence of the coating is lower than in the case of perpendicular thermal conductivity due to the high thermal conductivity of the CCs. The aging mechanisms occurring here are determined by $\overline{T}_{Ag}$ [3,4] and possible gradients in the electrolyte concentration caused by ΔT_{Cell} [50].

Particle cracking on the cathode side is more pronounced in regions at the higher than the lower local aging temperature $\overline{T}_{Ag}$. The extent is significantly lower than in the case of the through-plane gradients. The SEM images of the cathode cross-sections of IZ 10 – 40 °C in Fig. 6 and of IY 10 – 40 °C in Fig. S6 in the supplementary information explain the difference in the values of the effective thermal conductivity for the different sample positions in each cell. This shows that the through-plane gradient between 10 °C and 40 °C has a more severe impact on the changes of the microstructure and thus also of the thermophysical properties for the cathode than the in-plane gradient IY 10 – 40 °C. In the case of the global in-plane gradient over the cell of IY 30 – 50 °C, homogeneous changes of the thermophysical material properties arise during aging that correspond to the values of the through-plane gradient IZ 30 – 50 °C. This leads to the conclusion that the through-plane gradient must be sufficiently high to generate additional effects and induce inhomogeneous changes in the thermophysical properties in comparison to the in-plane temperature gradient or the homogeneous aging conditions with the equivalent mean cell aging temperature.

On the anode side, plating occurs increasingly on the cooler side of the in-plane gradient near the tab, also reported in the literature by Xie et al. [51]. As has already been analyzed for the through-plane gradient, plating on the anode side has no reducing influence on the effective thermal conductivity. There appears to be a significant change between the in- and through-plane direction for the gradient with the temperature difference between 30 °C and 50 °C, confirming the results of the cathodes investigated. Regarding the anodes, however, $\overline{T}_{Ag}$ is more decisive for the changes of the effective thermal conductivity during aging and a higher $\overline{T}_{Ag}$ may lead to increased solid heat conduction paths due to the stronger SEI growth. This results in inhomogeneous thermophysical properties for the anode, regardless of the size of ΔT_{Cell}. In comparison to the homogeneous results from HS 45 °C and HS 48 °C a reduction of the effective thermal conductivity for the inhomogeneous cells can be observed. The presence of the gradient leads to additional aging effects, which reduces the effective thermal conductivity. Regarding the in-plane gradient IY 10 – 40 °C the effect of the gradient direction observed for the cathode, with a significant smaller impact of the in-plane compared to the through-plane direction, is also confirmed for the anode.

5. Conclusion

In summary, the influences of various inhomogeneous thermal aging conditions on the thermophysical properties of cathodes and anodes are experimentally investigated and presented in this paper. The results include reference to the thermophysical properties of homogeneous thermal aging conditions and the values at the BoL for a commercial 20 Ah pouch cell (NMC-LCO blend cathode and graphite anode). A post-mortem analysis was performed to analyze any microstructural changes. The results of this study enable to differentiate between the influence of the local average aging temperature $\overline{T}_{Ag}$ and the additional influences of a thermal gradient over the cell with a temperature difference ΔT_{Cell} regarding the gradient direction and the local gradient over the individual electrodes with a temperature difference ΔT_{Local}.

It is shown that anode and cathode exhibit a significantly different behavior considering the changes in the thermophysical properties during aging depending on $\overline{T}_{Ag}$. In the case of the cathode investigated, a higher $\overline{T}_{Ag}$ leads to a greater reduction in thermal conductivity. Concerning the anode investigated, a lower $\overline{T}_{Ag}$ leads to a greater reduction in the effective thermal conductivity.

Regarding the influence of temperature gradients over the cell ΔT_{Cell} on the aging-induced changes, the results show that the gradient direction is very important, with the through-plane temperature gradients having a stronger influence on the reduction of the effective thermal conductivity of anode and cathode during aging than the in-plane gradients. In addition, the through-plane gradient can show a self-reinforcing effect on the level of ΔT_{Local}.

The investigations show that not only $\overline{T}_{Ag}$, but also the combined effects of ΔT_{Cell} and ΔT_{Local} must be considered. The following key findings can be drawn from the results of the thermal gradients investigated:

- Inhomogeneous thermal aging conditions can induce inhomogeneous thermophysical properties of the anode and cathode. A lower $\overline{T}_{Ag}$ is the more critical condition for the anode investigated and a higher $\overline{T}_{Ag}$ for the cathode investigated.
- It was found that a high enough through-plane temperature gradient across the entire cell with ΔT_{Cell} must be present for the pronounced inhomogeneous changes.
- A sufficiently large through-plane gradient results in a self-reinforcing effect of reducing the effective thermal conductivity of the electrodes. Due to the reduction of the effective thermal conductivity during aging, the local temperature gradient and therefore ΔT_{Local} can increase.

Due to the significant changes in the thermophysical properties of the anode and cathode compared to the BoL and the realization that self-reinforcing behavior can occur due to through-plane gradients, aged thermophysical properties should be considered when designing BTMS and second life applications. The changes in the thermal behavior of the battery electrodes are determined not only by the overall SoH or the average aging temperature of the cell, but also significantly by the thermal boundary conditions given, temperature distribution occurring within the cells and the direction of the temperature gradients. This classification of the three levels of impact can also be applied to other cell designs and chemistries, but the respective characteristics of the aging mechanisms and the associated effect on the thermophysical properties cannot be directly transferred.

The aging-induced changes in thermophysical parameters should also be further investigated in the future incorporating additional aging conditions and extensive analysis for the correlation with the underlying aging effects as well as targeting further cell chemistries for a deeper understanding. Another aspect is the transfer to the cell level. Further investigations are necessary to assess the effects of these local changes in electrode properties on the overall cell behavior and to make predictions about thermophysical properties based on aging. In addition, the influence of possible electrolyte dry-out on the thermophysical properties can be investigated at cell level.

CRediT authorship contribution statement

Leonie Pfeifer: Writing – review & editing, Writing – original draft, Visualization, Validation, Project administration, Methodology, Investigation, Formal analysis, Data curation, Conceptualization. **Sabrina Herberger:** Methodology, Investigation, Formal analysis. **Thomas Wetzel:** Writing – review & editing, Supervision, Resources, Project administration, Funding acquisition. **Philipp Seegert:** Writing – review & editing, Supervision, Resources, Project administration, Methodology, Funding acquisition, Conceptualization.

Declaration of competing interest

The authors declare that they have no known competing financial interests or personal relationships that could have appeared to influence the work reported in this paper.

Acknowledgements

We gratefully acknowledge the funding and support by the German Research Foundation (DFG) within the research training group SiMET under the project number 281041241/GRK2218. The authors would also like to especially thank Marcus Müller (KIT, IAM-ESS) for conducting the SEM and EDX measurements and the valuable discussions as well as Monika Raab (IAM-ESS) for the mercury porosimetry measurements. For their support with parts of the cell openings for this work the authors would like to thank Lisa Cloos (KIT, TVT), Marc Schiffler (KIT, IAM-ET) and Andre Weber (KIT, IAM-ET).

Appendix A. Supplementary data

Supplementary data to this article can be found online at https://doi.org/10.1016/j.jpowsour.2026.239620.

Data availability

Data will be made available on request.

References

[1] D. Werner, S. Paarmann, A. Wiebelt, T. Wetzel, Inhomogeneous temperature distribution affecting the cyclic aging of Li-Ion cells. Part II: analysis and correlation, Batteries 6 (2020) 12, https://doi.org/10.3390/batteries6010012.
[2] D. Werner, S. Paarmann, T. Wetzel, Calendar aging of Li-Ion cells—experimental investigation and empirical correlation, Batteries 7 (2021) 28, https://doi.org/10.3390/batteries7020028.
[3] S. Paarmann, K. Schuld, T. Wetzel, Inhomogeneous aging in lithium-ion batteries caused by temperature effects, Energ. Tech. 10 (2022) 2200384, https://doi.org/10.1002/ente.202200384.
[4] L. Cloos, T. Wetzel, In-plane versus through-plane thermal gradients during cyclic aging of lithium-ion batteries: an experimental study, Energ. Tech. (2025) 2402409, https://doi.org/10.1002/ente.202402409.
[5] R. Carter, T.A. Kingston, R.W. Atkinson, M. Parmananda, M. Dubarry, C. Fear, P. P. Mukherjee, C.T. Love, Directionality of thermal gradients in lithium-ion batteries dictates diverging degradation modes, Cell Rep. Phys. Sci. 2 (2021) 100351, https://doi.org/10.1016/j.xcrp.2021.100351.
[6] Y. Troxler, B. Wu, M. Marinescu, V. Yufit, Y. Patel, A.J. Marquis, N.P. Brandon, G. J. Offer, The effect of thermal gradients on the performance of lithium-ion batteries, J. Power Sources 247 (2014) 1018–1025, https://doi.org/10.1016/j.jpowsour.2013.06.084.
[7] S. Li, C. Zhang, Y. Zhao, G.J. Offer, M. Marinescu, Effect of thermal gradients on inhomogeneous degradation in lithium-ion batteries, Commun. Eng. 2 (2023) 74, https://doi.org/10.1038/s44172-023-00124-w.
[8] S. Paarmann, How Non-uniform Temperatures Influence the Performance and Ageing of Lithium-Ion Batteries, (n.d.).
[9] J.S. Edge, S. O'Kane, R. Prosser, N.D. Kirkaldy, A.N. Patel, A. Hales, A. Ghosh, W. Ai, J. Chen, J. Yang, S. Li, M.-C. Pang, L. Bravo Diaz, A. Tomaszewska, M. W. Marzook, K.N. Radhakrishnan, H. Wang, Y. Patel, B. Wu, G.J. Offer, Lithium ion battery degradation: what you need to know, Phys. Chem. Chem. Phys. 23 (2021) 8200–8221, https://doi.org/10.1039/D1CP00359C.
[10] M. Fleckenstein, O. Bohlen, B. Bäker, Aging effect of temperature gradients in Li-ion cells experimental and simulative investigations and the consequences on thermal battery management, WEVJ 5 (2012) 322–333, https://doi.org/10.3390/wevj5020322.
[11] I.A. Hunt, Y. Zhao, Y. Patel, J. Offer, Surface cooling causes accelerated degradation compared to tab cooling for lithium-ion pouch cells, J. Electrochem. Soc. 163 (2016) A1846–A1852, https://doi.org/10.1149/2.0361609jes.
[12] L. Spitthoff, P.R. Shearing, O.S. Burheim, Temperature, ageing and thermal management of lithium-ion batteries, Energies 14 (2021) 1248, https://doi.org/10.3390/en14051248.
[13] L. Tendera, D. Wycisk, C. Gonzalez, J. Stadler, K.P. Birke, Influence of state of health and individual aging mechanisms on the thermal conductivity of lithium-ion cells, J. Energy Storage 62 (2023) 106940, https://doi.org/10.1016/j.est.2023.106940.
[14] L. Tendera, D. Wycisk, C. Gonzalez, G.K. Mertin, H. Pegel, K.P. Birke, Effects of geometric, structural and operational parameters on the thermal conductivity of lithium-ion cells, J. Power Sources 549 (2022) 232120, https://doi.org/10.1016/j.jpowsour.2022.232120.
[15] A. Marconnet, S. Herberger, S. Paarmann, P. Seegert, T. Wetzel, Impact of aging on the thermophysical properties of lithium-ion battery electrodes, J. Power Sources 603 (2024) 234367, https://doi.org/10.1016/j.jpowsour.2024.234367.
[16] L. Spitthoff, M.S. Wahl, P.J.S. Vie, O.S. Burheim, Thermal transport in lithium-ion batteries: the effect of degradation, J. Power Sources 577 (2023) 233149, https://doi.org/10.1016/j.jpowsour.2023.233149.
[17] L. Cloos, J. Langer, M. Schiffler, A. Weber, Th. Wetzel, challenges of predicting temperature dependent capacity loss using the example of NMC-LMO lithium-ion

battery cells, J. Electrochem. Soc. 171 (2024) 040538, https://doi.org/10.1149/1945-7111/ad3ec3.
[18] D. Oehler, Bestimmung der thermischen Transporteigenschaften poröser Elektroden von Lithium-Ionen Batterien. https://doi.org/10.5445/KSP/1000136047, 2021.
[19] D. Oehler, J. Bender, P. Seegert, T. Wetzel, Investigation of the effective thermal conductivity of cell stacks of li-ion batteries, Energ. Tech. 9 (2021) 2000722, https://doi.org/10.1002/ente.202000722.
[20] L. Cloos, Aging of lithium-ion batteries under complex thermal conditions. https://doi.org/10.5445/IR/1000189128, 2025.
[21] P. Stephan, S. Kabelac, M. Kind, D. Mewes, K. Schaber, T. Wetzel (Eds.), VDI-Wärmeatlas: Fachlicher Träger VDI-Gesellschaft Verfahrenstechnik Und Chemieingenieurwesen, Springer Berlin Heidelberg, Berlin, Heidelberg, 2019, https://doi.org/10.1007/978-3-662-52989-8.
[22] A. Loges, S. Herberger, D. Werner, T. Wetzel, Thermal characterization of Li-ion cell electrodes by photothermal deflection spectroscopy, J. Power Sources 325 (2016) 104–115, https://doi.org/10.1016/j.jpowsour.2016.05.082.
[23] R.L. McMasters, J.V. Beck, R.B. Dinwiddie, H. Wang, Accounting for penetration of laser heating in flash thermal diffusivity experiments, J. Heat Tran. 121 (1999) 15–21, https://doi.org/10.1115/1.2825929.
[24] BIPM, IEC, IFCC, ILAC, ISO, IUPAC, IUPAP, and OIML, Evaluation of measurement data - guide to the expression of uncertainty in measurement. Joint Committee for Guides in Metrology, (n.d.). https://www.bipm.org/documents/20126/2071204/JCGM_100_2008_E.pdf/(accessed January 24, 2024).
[25] M. Steinhardt, J.V. Barreras, H. Ruan, B. Wu, G.J. Offer, A. Jossen, Meta-analysis of experimental results for heat capacity and thermal conductivity in lithium-ion batteries: a critical review, J. Power Sources 522 (2022) 230829, https://doi.org/10.1016/j.jpowsour.2021.230829.
[26] A. Friesen, X. Mönnighoff, M. Börner, J. Haetge, F.M. Schappacher, M. Winter, Influence of temperature on the aging behavior of 18650-type lithium ion cells: a comprehensive approach combining electrochemical characterization and post-mortem analysis, J. Power Sources 342 (2017) 88–97, https://doi.org/10.1016/j.jpowsour.2016.12.040.
[27] G. Qian, Y. Zhang, L. Li, R. Zhang, J. Xu, Z. Cheng, S. Xie, H. Wang, Q. Rao, Y. He, Y. Shen, L. Chen, M. Tang, Z.-F. Ma, Single-crystal nickel-rich layered-oxide battery cathode materials: synthesis, electrochemistry, and intra-granular fracture, Energy Storage Mater. 27 (2020) 140–149, https://doi.org/10.1016/j.ensm.2020.01.027.
[28] H. Li, A. Liu, N. Zhang, Y. Wang, S. Yin, H. Wu, J.R. Dahn, An unavoidable challenge for Ni-Rich positive electrode materials for lithium-ion batteries, Chem. Mater. 31 (2019) 7574–7583, https://doi.org/10.1021/acs.chemmater.9b02372.
[29] H. Ryu, G. Park, C.S. Yoon, Y. Sun, Microstructural degradation of Ni-Rich Li[Ni $_x$ Co $_y$ Mn $_{1-x-y}$]O $_2$ cathodes during Accelerated Calendar aging, Small 14 (2018) 1803179, https://doi.org/10.1002/smll.201803179.
[30] H. Liu, J.M. Foster, A. Gully, S. Krachkovskiy, M. Jiang, Y. Wu, X. Yang, B. Protas, G.R. Goward, G.A. Botton, Three-dimensional investigation of cycling-induced microstructural changes in lithium-ion battery cathodes using focused ion beam/scanning electron microscopy, J. Power Sources 306 (2016) 300–308, https://doi.org/10.1016/j.jpowsour.2015.11.108.
[31] P. Yan, J. Zheng, M. Gu, J. Xiao, J.-G. Zhang, C.-M. Wang, Intragranular cracking as a critical barrier for high-voltage usage of layer-structured cathode for lithium-ion batteries, Nat. Commun. 8 (2017), https://doi.org/10.1038/ncomms14101.
[32] Y. Ruan, X. Song, Y. Fu, C. Song, V. Battaglia, Structural evolution and capacity degradation mechanism of LiNi0.6Mn0.2Co0.2O2 cathode materials, J. Power Sources 400 (2018) 539–548, https://doi.org/10.1016/j.jpowsour.2018.08.056.
[33] T. Yoon, S. Park, J. Mun, J.H. Ryu, W. Choi, Y.-S. Kang, J.-H. Park, S.M. Oh, Failure mechanisms of LiNi0.5Mn1.5O4 electrode at elevated temperature, J. Power Sources 215 (2012) 312–316, https://doi.org/10.1016/j.jpowsour.2012.04.103.
[34] B.S. Parimalam, A.D. MacIntosh, R. Kadam, B.L. Lucht, Decomposition reactions of anode Solid electrolyte interphase (SEI) components with $LiPF_6$, J. Phys. Chem. C 121 (2017) 22733–22738, https://doi.org/10.1021/acs.jpcc.7b08433.
[35] M. Storch, S.L. Hahn, J. Stadler, R. Swaminathan, D. Vrankovic, C. Krupp, R. Riedel, Post-mortem analysis of calendar aged large-format lithium-ion cells: investigation of the solid electrolyte interphase, J. Power Sources 443 (2019) 227243, https://doi.org/10.1016/j.jpowsour.2019.227243.
[36] B. Stiaszny, J.C. Ziegler, E.E. Krauß, J.P. Schmidt, E. Ivers-Tiffée, Electrochemical characterization and post-mortem analysis of aged LiMn2O4–Li(Ni0.5Mn0.3Co0.2)O2/graphite lithium ion batteries. Part I: cycle aging, J. Power Sources 251 (2014) 439–450, https://doi.org/10.1016/j.jpowsour.2013.11.080.
[37] X. Han, M. Ouyang, L. Lu, J. Li, Y. Zheng, Z. Li, A comparative study of commercial lithium ion battery cycle life in electrical vehicle: aging mechanism identification, J. Power Sources 251 (2014) 38–54, https://doi.org/10.1016/j.jpowsour.2013.11.029.
[38] J. Chen, J. Liu, Y. Qi, T. Sun, X. Li, Unveiling the roles of binder in the mechanical integrity of electrodes for lithium-ion batteries, J. Electrochem. Soc. 160 (2013) A1502–A1509, https://doi.org/10.1149/2.088309jes.
[39] J.R. Belt, C.D. Ho, T.J. Miller, M.A. Habib, T.Q. Duong, The effect of temperature on capacity and power in cycled lithium ion batteries, J. Power Sources 142 (2005) 354–360, https://doi.org/10.1016/j.jpowsour.2004.10.029.
[40] S. Paarmann, L. Cloos, J. Technau, T. Wetzel, Measurement of the temperature influence on the current distribution in lithium-ion batteries, Energ. Tech. 9 (2021) 2000862, https://doi.org/10.1002/ente.202000862.
[41] W. Waag, S. Käbitz, D.U. Sauer, Experimental investigation of the lithium-ion battery impedance characteristic at various conditions and aging states and its influence on the application, Appl. Energy 102 (2013) 885–897, https://doi.org/10.1016/j.apenergy.2012.09.030.
[42] R. Carter, C.T. Love, Modulation of lithium plating in Li-Ion batteries with external thermal gradient, ACS Appl. Mater. Interfaces 10 (2018) 26328–26334, https://doi.org/10.1021/acsami.8b09131.
[43] O. Krischer, W. Kast, O. Krischer, Die Wissenschaftlichen Grundlagen Der Trocknungstechnik, 3., Neubearb. Aufl, Springer, Berlin ; New York, 1978.
[44] F. Richter, S. Kjelstrup, P.J.S. Vie, O.S. Burheim, Thermal conductivity and internal temperature profiles of Li-ion secondary batteries, J. Power Sources 359 (2017) 592–600, https://doi.org/10.1016/j.jpowsour.2017.05.045.
[45] L. Cloos, S. Herberger, P. Seegert, T. Wetzel, Thermal material properties of commercial NMC111-LMO/graphite lithium-ion battery cell. https://doi.org/10.35097/KALRZQZUAHBXWKIJ, 2024.
[46] J. Schmalstieg, Physikalisch-elektrochemische Simulation Von Lithium-Ionen-Batterien : Implementierung, Parametrierung Und Anwendung, RWTH Aachen University, 2017, https://doi.org/10.18154/RWTH-2017-04693.
[47] S.J. Harris, A. Timmons, D.R. Baker, C. Monroe, Direct in situ measurements of li transport in Li-ion battery negative electrodes, Chem. Phys. Lett. (2010).
[48] Y. Dong, C. Liu, M. Rui, X. Zhang, Y. Guan, L. Chen, Q. Huang, M. Wang, Y. Su, F. Wu, N. Li, Review on graphite anodes for fast-charging lithium-ion batteries: mechanism, modification and characterizations, Adv. Funct. Mater. (2025), https://doi.org/10.1002/adfm.202506190.
[49] D. Burow, K. Sergeeva, S. Calles, K. Schorb, A. Börger, C. Roth, P. Heitjans, Inhomogeneous degradation of graphite anodes in automotive lithium ion batteries under low-temperature pulse cycling conditions, J. Power Sources 307 (2016) 806–814, https://doi.org/10.1016/j.jpowsour.2016.01.033.
[50] L. Ni, H. Ruan, Y. Zhang, Influence of thermal management and battery design on inhomogeneous lithium plating during fast charging, J. Power Sources 633 (2025) 236410, https://doi.org/10.1016/j.jpowsour.2025.236410.
[51] Y. Xie, S. Wang, R. Li, D. Ren, M. Yi, C. Xu, X. Han, L. Lu, B. Friess, G. Offer, M. Ouyang, Inhomogeneous degradation induced by lithium plating in a large-format lithium-ion battery, J. Power Sources 542 (2022) 231753, https://doi.org/10.1016/j.jpowsour.2022.231753.